Editors' Suggestion

Doping-Induced Second-Harmonic Generation in Centrosymmetric Graphene from Quadrupole Response

Yu Zhang,[1] Di Huang,[1] Yuwei Shan,[1] Tao Jiang,[1] Zhihong Zhang,[2] Kaihui Liu,[2] Lei Shi,[1,3] Jinluo Cheng,[4] John E. Sipe,[5] Wei-Tao Liu,[1,3,*] and Shiwei Wu[1,3,†]

[1]State Key Laboratory of Surface Physics, Key Laboratory of Micro and Nano Photonic Structures (MOE), Department of Physics, and Institute for Nanoelectronic Devices and Quantum Computing, Fudan University, Shanghai 200433, China
[2]State Key Laboratory for Mesoscopic Physics and School of Physics, Peking University, Beijing 100871, China
[3]Collaborative Innovation Center of Advanced Microstructures, Nanjing 210093, China
[4]Changchun Institute of Optics, Fine Mechanics and Physics, Chinese Academy of Sciences, Changchun, Jilin 130033, China
[5]Department of Physics, University of Toronto, Toronto, Ontario M5S 1A7, Canada

(Received 24 October 2018; published 28 January 2019)

For centrosymmetric materials such as monolayer graphene, no optical second-harmonic generation (SHG) is generally expected, because it is forbidden under the electric-dipole approximation. Yet we observe a strong, doping-induced SHG from graphene, with its highest strength comparable to the electric-dipole-allowed SHG in noncentrosymmetric 2D materials. This novel SHG has the nature of an electric-quadrupole response, arising from the effective breaking of inversion symmetry by optical dressing with an in-plane photon wave vector. More remarkably, the SHG is widely tuned by carrier doping or chemical potential, being sharply enhanced at Fermi-edge resonances but vanishing at the charge neutral point that manifests the electron-hole symmetry of massless Dirac fermions. This striking behavior in graphene, which should also arise in graphenelike Dirac materials, expands the scope of nonlinear optics and holds the promise of novel optoelectronic and photonic applications.

DOI: 10.1103/PhysRevLett.122.047401

Second-harmonic generation (SHG) is the most fundamental second-order nonlinear optical process, described by $\mathbf{P}(2\omega = \omega + \omega) = \chi^{(2)}(\omega, \mathbf{q}) : \mathbf{E}(\omega)\mathbf{E}(\omega)$ [1]. In this process, the output signal is frequency doubled from the incident photon field of $\mathbf{E}(\omega)$. Here, $\chi^{(2)}(\omega, \mathbf{q})$ is the rank-three nonlinear susceptibility tensor and depends on the incident frequency ω and photon wave vector $\mathbf{q}$. Since $\mathbf{q}$ is typically small, a Taylor expansion yields $\chi^{(2)}(\omega, \mathbf{q}) \approx \chi^{(2)}_{\mathrm{ED}}(\omega) + \chi^{(3)}_{\mathrm{EQ}}(\omega)\mathbf{q} + o(\mathbf{q}^2)$. $\chi^{(2)}_{\mathrm{ED}}(\omega)$ is the leading electric-dipole (ED) term, and $\chi^{(3)}_{\mathrm{EQ}}(\omega)$ is the often-neglected electric-quadrupole or magnetic-dipole term [1,2] or the EQ response for simplicity. For the electric-dipole-allowed SHG to exist, the breaking of inversion symmetry is essential. Hence, SHG is a sensitive probe of symmetry-governed phenomena such as ferroelectricity [3], valley pseudospin [4], and phase transitions [5].

For 2D materials such as hexagonal boron nitride, transition metal dichalcogenide, and monochalcogenide, the atomic lattices in monolayer form are noncentrosymmetric, giving rise to the electric-dipole-allowed SHG. In fact, SHG has become an indispensable tool to characterize their crystal orientation, stacking symmetry, and electronic features [6–10]. Yet, for an isolated monolayer graphene, it is centrosymmetric and no electric-dipole SHG is allowed. The third-order optical nonlinearity such as third-harmonic generation [11–15] and four-wave mixing [14,16] was often regarded as the dominant nonlinear process in graphene. Only weak SHG was observed on supported monolayers, which was attributed to the inversion symmetry breaking by the underlying substrate [17] or an in-plane electric current [18,19]. Therefore, graphene provides a unique platform to study unusual SHG responses such as valley polarization-induced SHG [20,21] and the EQ response beyond the electric-dipole approximation [22,23], as theoretically proposed.

In this work, we exclusively investigate the EQ response of SHG in graphene by introducing an in-plane photon wave vector $\mathbf{q}$ at oblique incidence, which effectively breaks the overall inversion symmetry of the system [22–25]. By comparing with the SHG response at normal incidence, we could exclude other possible origins such as the substrate-induced SHG [17]. More importantly, we find that the EQ response of SHG in graphene is widely tunable by carrier doping or chemical potential and exhibits strong Fermi-edge resonances, by using ion-gel electric gating [14]. The strong EQ SHG in graphene is even comparable to the ED-allowed SHG from noncentrosymmetric 2D materials with parabolic bands [6–8,10], and the effective nonlinear susceptibility is about 4 orders of magnitude stronger than the EQ response in bulk fused silica [26] (rarely reported for other materials). Furthermore, we find that this EQ process is intrinsically sensitive to the electron-hole symmetry of the energy bands, strictly vanishing at the zero chemical potential. In the past,

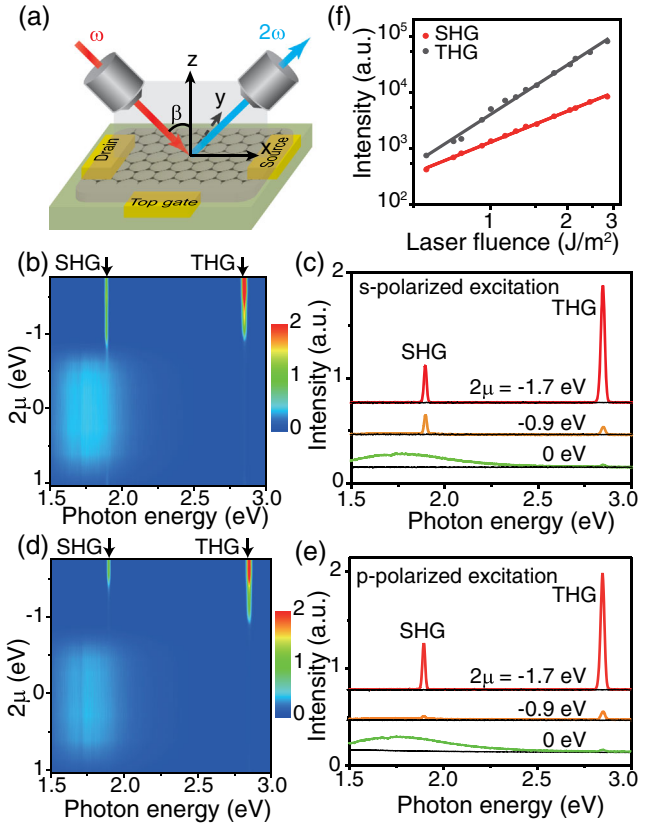

FIG. 1. SHG from ion-gel gated graphene with oblique incident excitation. (a) Experimental geometry at an oblique incidence of 45°. The graphene supported on a fused silica substrate is covered with ion gel for gating, through which the chemical potential μ could be tuned from −0.9 to 0.5 eV. The laser excitation and signal collection are done through microscope objectives with numerical apertures of 0.35 and 0.40, respectively. The incident photon energy was 0.95 eV, unless otherwise noted. (b) Specularly reflected spectra with s-polarized excitation as a function of 2μ. (c) Selected spectra in (b) at different chemical potentials μ. The spectra are offset for clarity. (d),(e) Corresponding spectra with the p-polarized excitation. The spectra from bare fused silica covered with ion gel at corresponding gate voltages are also shown as black lines in (c) and (e) for comparison. The broadband background at low doping is from the ultrafast nonlinear photoluminescence, which could be switched off at high doping [32,33]. The incident laser fluence was 2.4 J/m^2. (f) Incident fluence dependence of SHG (red) and THG (gray) intensities at a heavily doped level ($\mu \approx -0.88$ eV) on a double-logarithmic scale. Solid lines are fits with slopes of 1.85 ± 0.02 and 2.95 ± 0.06, respectively.

nonlinear optics have long been established as powerful tools for analyzing the space and time symmetries of materials [1,5–10]. Now we can add electron-hole symmetry to this family and utilize the EQ response to study related Dirac materials such as topological insulators [27] and Dirac and Weyl semimetals [28].

Our experimental geometry is sketched in Fig. 1(a), with the excitation beam ($\hbar\omega = 0.95$ eV, unless otherwise noted) incident at 45° from the surface normal of the ion-gel gated graphene [14]. The doping level or chemical potential in graphene could be electrically tuned by the gate voltage, and the relationship between the gate voltage and chemical potential was determined from the infrared transmittance spectra. Additional experimental details are provided in Ref. [14] as well as in Supplemental Material [29]. Along the direction of specular reflection, a signal at 2ω could be observed from graphene, which is vanishing with the chemical potential tuned toward the charge neutral point (CNP), but grows rapidly upon the increase of chemical potential $|\mu|$ [Figs. 1(b) and 1(c) for s-polarized incidence and Figs. 1(d) and 1(e) for p-polarized incidence]. In comparison, there is no observable SHG on the ion-gel-covered fused silica substrate at any gate voltage [black lines in Figs. 1(c) and 1(e)]. The signal intensity on graphene was proportional to the square of incident fluence [red symbols in Fig. 1(f)], confirming it to be an SHG response.

In earlier studies by Dean and van Driel [17], weak SHG was observed from pristine graphene monolayers at an oblique incidence of 60° and was attributed to the usual ED-type response due to the breaking of inversion symmetry by the presence of the oxidized silicon substrate. Since ED SHG and EQ SHG arise from different susceptibility tensors, they can be distinguished by varying the experimental geometry from the oblique incidence to normal incidence. If the SHG were purely of ED type, the signal at normal incidence should be comparable to that under the oblique geometry. If the EQ SHG dominates, a large intensity contrast between the two geometries would be expected, because an in-plane component of the photon wave vector is essential to the EQ SHG (see details in Supplemental Material [29]). We thus performed the SHG measurement under the normal incidence [Fig. 2(a)]. The signal is only about 0.6% of the oblique SHG at the same chemical potential [Fig. 2(b)], consistent with the dominance of EQ SHG.

The EQ SHG originates from the nonlinear polarization $\mathbf{P}_{\mathrm{EQ}}(2\omega) \propto \chi^{(3)}_{\mathrm{EQ}}\mathbf{q}\mathbf{E}(\omega)^2$. This relation imposes symmetry restrictions to the EQ SHG, which can be manifest in polarization features as displayed in Fig. 3. Because of the 2D geometry of graphene, we consider only the in-plane subset of $\chi^{(3)}_{\mathrm{EQ}}$ (full expression given in Supplemental Material [29]). Since graphene belongs to the point group D_{6h} $(6/mmm)$, this subset has an identical construction to that of an isotropic surface [1]; in other words, the graphene plane is optically isotropic for $\chi^{(3)}$ processes [14,31]. When the incident beam is p polarized, the incident plane defines a mirror plane of the system [Fig. 3(a)]. So $\mathbf{P}_{\mathrm{EQ}}(2\omega)$, which is a polar vector, must lie in the incident plane; otherwise, it would change sign after the mirror reflection and break the symmetry. When the incident beam is s polarized, the $\mathbf{E}(\omega)^2$ relation in the expression of $\mathbf{P}_{\mathrm{EQ}}(2\omega)$ again imposes a mirror symmetry along the incident plane, restricting

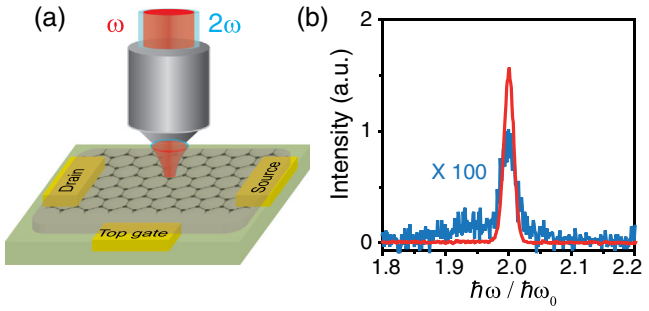

FIG. 2. Comparison of SHG between normal and oblique incidences. (a) Experimental geometry at normal incidence. The excitation and collection are through the same objective with a numerical aperture as high as 0.95. (b) SHG spectra from heavily doped graphene ($\mu = -0.8$ eV) at the same incident fluence of 2.4 J/m^2. The red and blue data represent the cases of oblique (s-polarized) and normal incidences, respectively. The spectrum at normal incidence is magnified by 100 times.

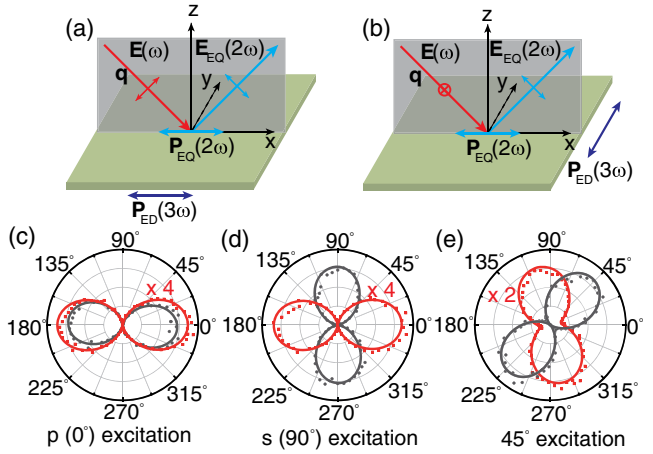

FIG. 3. Polarization characteristics of the SHG at an oblique incidence of 45°. (a),(b) Symmetry properties of the overall system defined by both the input electric field and wave vector. For both s- and p-polarized excitations, $\mathbf{P}_{\mathrm{EQ}}(2\omega)$ is confined in the mirror plane defined by the incident plane, while $\mathbf{P}_{\mathrm{ED}}(3\omega)$ follows the in-plane projection of $\mathbf{E}(\omega)$. (c)–(e) The SHG (red dots) intensity versus the angle θ between the beam incident plane and analyzer polarization direction, under at p-, s-, and 45°-polarized excitations, respectively. The THG (gray dots) data are also shown for comparison. Solid lines are fits using equations in Supplemental Material [29]. The graphene was heavily doped at $\mu = -0.88$ eV.

$\mathbf{P}_{\mathrm{EQ}}(2\omega)$ to remain in this plane [Fig. 3(b)]. Hence, the EQ SHG must be p polarized in both cases [22]. We verified that by changing the angle (θ) between the signal analyzer and the beam incident plane. As seen in Figs. 3(c) and 3(d) (red squares), for both p- and s-polarized excitations, the signal polarization patterns can be nicely fitted by the function $\cos^2\theta$, corresponding to a linearly p-polarized output.

On the other hand, if the incident beam has both p and s components, the EQ SHG is not a trivial superposition of two p-polarized fields but, in general, becomes elliptically polarized [22,23,25] [Fig. 3(e), red squares]. This is because there is no longer any mirror plane defined by $\mathbf{q}$ or $\mathbf{E}(\omega)$, so $\mathbf{P}_{\mathrm{EQ}}(2\omega)$ is not restricted to be along either of them. These behaviors are in contrast to the ED-type third-harmonic generation (THG) arising from $\mathbf{P}_{\mathrm{ED}}(3\omega) \propto \chi^{(3)}_{\mathrm{ED}}\mathbf{E}(\omega)^3$, which always has a mirror plane defined along $\mathbf{E}(\omega)$ and keeps $\mathbf{P}_{\mathrm{ED}}(3\omega)$ parallel to the in-plane projection of $\mathbf{E}(\omega)$ [Figs. 3(c)–3(e), gray dots] [14,31]. Detailed calculations based on EQ and ED types of $\chi^{(3)}$ tensors yielded nice fits to the polarization patterns of SHG and THG, respectively [solid lines in Figs. 3(c)–3(e)] (see Supplemental Material for details [29]).

We now discuss the prominent μ dependence of the EQ SHG [Fig. 4(a)]. The very weak SHG near $\mu = 0$ or the CNP grows rapidly as μ approaches the Fermi-edge resonances at one-photon ($2|\mu| = \hbar\omega$) and two-photon ($|\mu| = \hbar\omega$) energies [Fig. 4(b)]. Meanwhile, the s- and p-polarized excitations result in distinct line profiles [Fig. 4(a)], indicating that different tensor elements have different μ dependences. Throughout, the intensity could be tuned over 2 orders of magnitudes by electrically tuning the chemical potential μ. Theoretically, the μ dependence of EQ SHG has been predicted by the full quantum mechanical calculations by Wang, Tokman, and Belyanin [22] and Cheng, Vermeulen, and Sipe [23] and is attributed to the resonant transitions in the linearly dispersed band structure of graphene. As shown in Fig. 4(c), the calculation nicely reproduces the Fermi-edge resonances, as well as the relative strength between different tensor elements observed in our measurements [Fig. 4(a)]. The calculated magnitude of the effective second-order nonlinear susceptibility $|\chi^{(3)}_{\mathrm{EQ}}q_x|$ is also close to the experimental values.

As previously reported [14], the third-harmonic generation also grows with chemical potential μ and exhibits the Fermi-edge resonances (Fig. S1). On the other hand, there is a marked difference between the μ dependence of EQ SHG and ED THG. In contrast to the vanishing EQ SHG at $\mu = 0$, the THG is readily detectable as shown in Figs. 1(c) and 1(e). Accordingly, under the two-band approximation, the calculation shows that $\chi^{(3)}_{\mathrm{ED}}$ for THG and four-wave mixing are even functions of μ [31], but $\chi^{(3)}_{\mathrm{EQ}}$ for EQ SHG is an odd function with respect to μ that has to vanish at the CNP [22,23] [Figs. 4(d)–4(f)]. The latter is a direct consequence of the spatial dispersion for EQ-type responses, in combination with the electron-hole symmetry and time-reversal symmetry of graphene. The detailed proof is provided in Supplemental Material [29], and here we briefly sketch the physical picture. Each element of the optical susceptibility tensor is a summation of diagrams like the one in Fig. 4(g), which depicts a transition with a photon wave vector $\mathbf{q}$ on the right-hand side of the energy bands at a finite μ. Because of the electron-hole symmetry

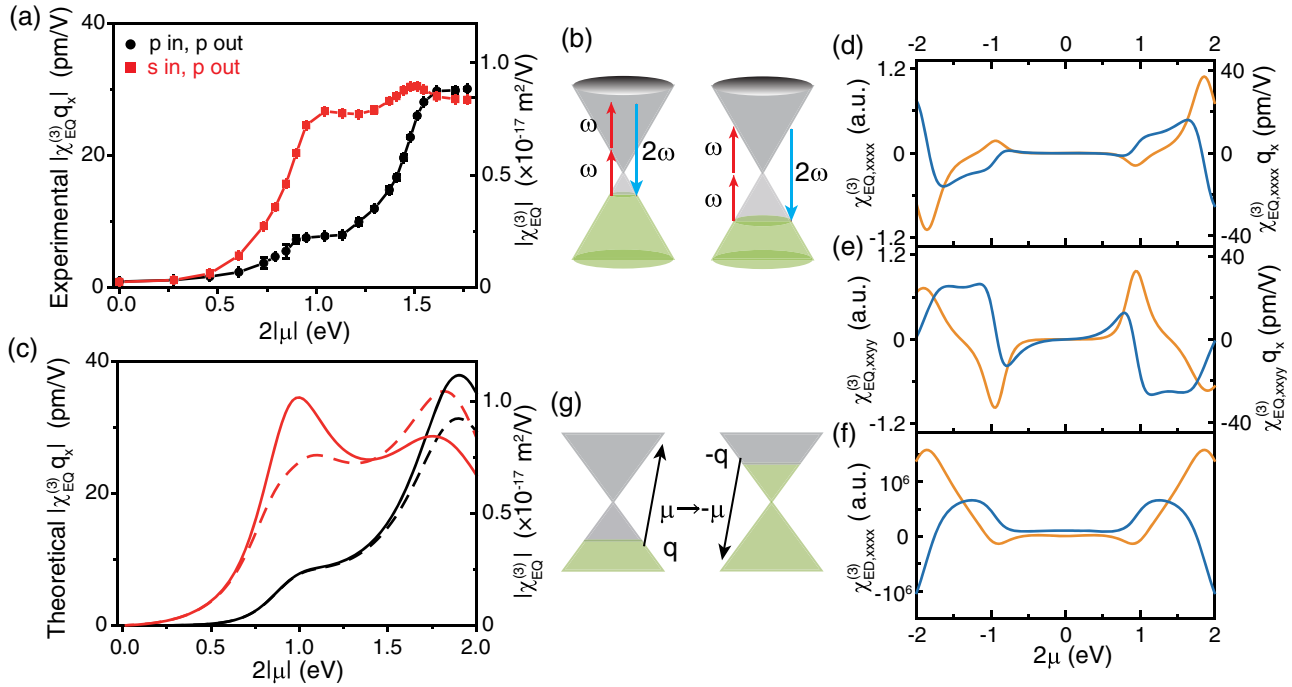

FIG. 4. Chemical potential dependence of the oblique SHG. (a) The extracted second-order nonlinear susceptibility $|\chi^{(3)}_{EQ} q_x|$ of the SHG under *s*- (red dots) and *p*-polarized (black dots) light excitation versus chemical potential $2|\mu|$. The data were extracted from Figs. 1(b) and 1(d) for negative chemical potentials. (b) Transition diagrams for one- and two-photon Fermi-edge resonances, respectively. (c) Theoretically calculated $|\chi^{(3)}_{EQ,xxyy} q_x|$ (red) and $|\chi^{(3)}_{EQ,xxxx} q_x|$ (black) for *s*- and *p*-polarized excitations, respectively. The dashed and solid lines are from the theories by Wang, Tokman, and Belyanin [22] and Cheng, Vermeulen, and Sipe [23], respectively. In the calculation, the temperature $T = 300$ K (ignoring the effect of high electron temperature for $2|\mu| \leq \hbar\omega$) and the resonant damping factor $\Gamma = 0.2|\mu|$eV are used [14]. (d),(e) Real (yellow) and imaginary (blue) parts of $\chi^{(3)}_{EQ,xxxx}$ and $\chi^{(3)}_{EQ,xxyy}$, corresponding to EQ SHG under *p*- and *s*-polarized excitations, respectively. On the right vertical axis, the effective second-order nonlinear susceptibilities $\chi^{(3)}_{EQ,xxxx} q_x$ and $\chi^{(3)}_{EQ,xxyy} q_x$ are also shown. (f) Real (yellow) and imaginary (blue) parts of $\chi^{(3)}_{ED,xxxx}$, corresponding to ED THG. The calculations were followed from the theory by Cheng, Vermeulen, and Sipe [23,31]. (g) Transition schematics under the operation of $\mu \to -\mu$ and $\mathbf{k} \to -\mathbf{k}$ with the electron-hole symmetry and time-reversal symmetry for $\mathbf{q} \to -\mathbf{q}$, where $\mathbf{k}$ is the electron wave vector and $\mathbf{q}$ the photon wave vector.

and time-reversal symmetry, the diagram is equivalent to a transition with $-\mathbf{q}$ on the left-hand side ($\mathbf{k} \to -\mathbf{k}$) for $\mu \to -\mu$. Therefore, the susceptibility tensor element at $\mathbf{q}$ and μ is equivalent to that at $-\mathbf{q}$ and $-\mu$. For the EQ SHG, each diagram contains a matrix element $\langle \mathbf{q} \rangle$; and, since $\langle -\mathbf{q} \rangle = -\langle \mathbf{q} \rangle$, we then have $\chi^{(3)}_{EQ}(\mu, \mathbf{q}) = \chi^{(3)}_{EQ}(-\mu, -\mathbf{q}) = -\chi^{(3)}_{EQ}(-\mu, \mathbf{q})$, which has an odd parity with respect to μ. This is fundamentally different from susceptibility for ED THG, which involves only matrix elements of dipole moments, and thus will not change sign upon the inversion of electron and hole bands.

Finally, we comment on the strength of EQ SHG in graphene. In conventional materials, the EQ SHG is often eclipsed by the ED-type counterpart. For example, the effective nonlinearity of the EQ response in fused silica is only about 4×10^{-3} pm/V [26]. Yet it can be exceptionally strong in graphene, reaching $|\chi^{(3)}_{EQ,xxyy} q_x| \sim 30$ pm/V upon Fermi-edge resonances for $\hbar\omega = 0.95$ eV. This is comparable to the ED-allowed $|\chi^{(2)}_{ED}|$ in noncentrosymmetric 2D materials such as *h*BN monolayer [8] and *ABA*-stacked trilayer graphene [9], which is typically about 10–100 pm/V. For TMDC monolayers such as MoS_2, the above $|\chi^{(2)}_{ED}|$ can increase by an order upon excitonic resonance [6,8,10] (Fig. S2). Nonetheless, such resonance is always accompanied by enhanced absorption and a lowered damage threshold. In contrast, the Fermi-edge resonances in graphene actually reduce the absorption, allowing graphene to be pumped at an even higher fluence for stronger responses. Moreover, as pointed out in Ref. [22], the dipole transition matrix element scales with ω^{-1} for the massless Dirac fermions in graphene, instead of $\omega^{-1/2}$ for conventional materials with the parabolic energy dispersion. We thus expect the EQ-type responses of graphene to have an even higher efficiency in the infrared frequency range. All these may explain the strong surface-plasmon-enhanced difference-frequency generation observed by Constant *et al.* [34] and Yao *et al.* [35]. Thus, the combination of an electrically tunable strong response and suppressed absorption damage makes

graphene a unique and highly promising candidate in nanophotonic and optoelectronic applications, ranging from optical rectification for terahertz generation to sum-frequency generation for parametric conversion.

In conclusion, we reveal in this work a doping-induced, strong SHG response from the centrosymmetric graphene monolayer, which has a comparable strength to that from noncentrosymmetric 2D materials. Based on its μ dependence, symmetry properties, and incident angle dependence, we attribute it to the EQ type of response resultant from the unique properties of massless Dirac fermions. Interestingly, we find that this EQ response is intrinsically sensitive to the electron-hole symmetry of the band structure, becoming strictly zero at the charge neutral point. The understanding derived here is readily applicable to other related Dirac materials such as topological insulators [27] and Dirac and Weyl semimetals [28]. Therefore, graphene provides a unique platform for investigating unusual nonlinear optical phenomena, which not only can expand the horizon of nonlinear optics in quantum materials but also has a large potential in novel device applications [35,36].

We thank Professor Yuen-Ron Shen for insightful discussion. The work at Fudan University was supported by the National Basic Research Program of China (Grant No. 2014CB921601), National Key Research and Development Program of China (Grants No. 2016YFA0301002 and No. 2016YFA0300900), National Natural Science Foundation of China (Grants No. 91421108, No. 11622429, and No. 11374065), and the Science and Technology Commission of Shanghai Municipality (Grant No. 16JC1400401). Part of the sample fabrication was performed at Fudan Nano-fabrication Laboratory. W.-T. L. is also supported from the National Program for Support of Top-Notch Young Professionals and the Shu Guang Project. K. L. is supported by National Natural Science Foundation of China (Grant No. 51522201). J. C. is supported by National Natural Science Foundation of China (Grant No. 11774340). J. E. S. is supported by the Natural Sciences and Engineering Research Council of Canada.

Y. Z. and D. H. equally contributed to this work.

*Corresponding author.
wtliu@fudan.edu.cn
†Corresponding author.
swwu@fudan.edu.cn

[1] Y. R. Shen, *The Principles of Nonlinear Optics* (Wiley-Interscience, New York, 1984).
[2] P. Yu and M. Cardona, *Fundamentals of Semiconductors: Physics and Materials Properties* (Springer, Berlin, 2010).
[3] W. Wu *et al.*, Piezoelectricity of single-atomic-layer MoS_2 for energy conversion and piezotronics, Nature (London) **514**, 470 (2014).
[4] D. Xiao, W. Yao, and Q. Niu, Valley-Contrasting Physics in Graphene: Magnetic Moment and Topological Transport, Phys. Rev. Lett. **99**, 236809 (2007).
[5] L. Zhao, C. A. Belvin, R. Liang, D. A. Bonn, W. N. Hardy, N. P. Armitage, and D. Hsieh, A global inversion-symmetry-broken phase inside the pseudogap region of $YBa_2Cu_3O_y$, Nat. Phys. **13**, 250 (2017).
[6] T. Jiang, H. Liu, D. Huang, S. Zhang, Y. Li, X. Gong, Y.-R. Shen, W.-T. Liu, and S. Wu, Valley and band structure engineering of folded MoS2 bilayers, Nat. Nanotechnol. **9**, 825 (2014).
[7] X. Zhou, J. Cheng, Y. Zhou, T. Cao, H. Hong, Z. Liao, S. Wu, H. Peng, K. Liu, and D. Yu, Strong second-harmonic generation in atomic layered GaSe, J. Am. Chem. Soc. **137**, 7994 (2015).
[8] Y. Li, Y. Rao, K. F. Mak, Y. You, S. Wang, C. R. Dean, and T. F. Heinz, Probing symmetry properties of few-layer MoS_2 and h-BN by optical second-harmonic generation, Nano Lett. **13**, 3329 (2013).
[9] Y. Shan Y. Li, D. Huang, Q. Tong, W. Yao, W.-T. Liu and S. Wu, Stacking symmetry governed second harmonic generation in graphene trilayers, Sci. Adv. **4**, eaat0074 (2018).
[10] C. Janisch, Y. Wang, D. Ma, N. Mehta, A. L. Elías, N. Perea-López, M. Terrones, V. Crespi, and Z. Liu, Extraordinary second harmonic generation in tungsten disulfide monolayers, Sci. Rep. **4**, 5530 (2014).
[11] S. A. Mikhailov, Non-linear electromagnetic response of graphene, Europhys. Lett. **79**, 27002 (2007).
[12] N. Kumar, J. Kumar, C. Gerstenkorn, R. Wang, H.-Y. Chiu, A. L. Smirl, and H. Zhao, Third harmonic generation in graphene and few-layer graphite films, Phys. Rev. B **87**, 121406 (2013).
[13] S.-Y. Hong, J. I. Dadap, N. Petrone, P.-C. Yeh, J. Hone, and R. M. Osgood, Jr., Optical Third-Harmonic Generation in Graphene, Phys. Rev. X **3**, 021014 (2013).
[14] T. Jiang *et al.*, Gate-tunable third-order nonlinear optical response of massless Dirac fermions in graphene, Nat. Photonics **12**, 430 (2018).
[15] G. Soavi *et al.*, Broadband, electrically tunable third-harmonic generation in graphene, Nat. Nanotechnol. **13**, 583 (2018).
[16] E. Hendry, P. J. Hale, J. Moger, A. K. Savchenko, and S. A. Mikhailov, Coherent Nonlinear Optical Response of Graphene, Phys. Rev. Lett. **105**, 097401 (2010).
[17] J. J. Dean and H. M. van Driel, Second harmonic generation from graphene and graphitic films, Appl. Phys. Lett. **95**, 261910 (2009).
[18] A. Y. Bykov, T. V. Murzina, M. G. Rybin, and E. D. Obraztsova, Second harmonic generation in multilayer graphene induced by direct electric current, Phys. Rev. B **85**, 121413 (2012).
[19] Y. Q. An, F. Nelson, J. U. Lee, and A. C. Diebold, Enhanced optical second-harmonic generation from the current-biased graphene/SiO_2/Si(001) structure, Nano Lett. **13**, 2104 (2013).
[20] T. O. Wehling, A. Huber, A. I. Lichtenstein, and M. I. Katsnelson, Probing of valley polarization in graphene via optical second-harmonic generation, Phys. Rev. B **91**, 041404 (2015).

[21] L. E. Golub and S. A. Tarasenko, Valley polarization induced second harmonic generation in graphene, Phys. Rev. B **90**, 201402 (2014).
[22] Y. Wang, M. Tokman, and A. Belyanin, Second-order nonlinear optical response of graphene, Phys. Rev. B **94**, 195442 (2016).
[23] J. L. Cheng, N. Vermeulen, and J. E. Sipe, Second order optical nonlinearity of graphene due to electric quadrupole and magnetic dipole effects, Sci. Rep. **7**, 43843 (2017).
[24] M. M. Glazov and S. D. Ganichev, High frequency electric field induced nonlinear effects in graphene, Phys. Rep. **535**, 101 (2014).
[25] M. M. Glazov, Second harmonic generation in graphene, JETP Lett. **93**, 366 (2011).
[26] X. Wei, S.-C. Hong, A. I. Lvovsky, H. Held, and Y. R. Shen, Evaluation of surface vs bulk contributions in sum-frequency vibrational spectroscopy using reflection and transmission geometries, J. Phys. Chem. B **104**, 3349 (2000).
[27] F. Giorgianni *et al.*, Strong nonlinear terahertz response induced by Dirac surface states in Bi_2Se_3 topological insulator, Nat. Commun. **7**, 11421 (2016).
[28] L. Wu, S. Patankar, T. Morimoto, N. L. Nair, E. Thewalt, A. Little, J. G. Analytis, J. E. Moore, and J. Orenstein, Giant anisotropic nonlinear optical response in transition metal monopnictide Weyl semimetals, Nat. Phys. **13**, 350 (2017).
[29] See Supplemental Material at http://link.aps.org/supplemental/10.1103/PhysRevLett.122.047401 for additional experimental details and theoretical analysis, which includes Refs. [30,31].
[30] X. Xu *et al.*, Ultrafast growth of single-crystal graphene assisted by a continuous oxygen supply, Nat. Nanotechnol. **11**, 930 (2016).
[31] J. L. Cheng, N. Vermeulen, and J. E. Sipe, Third order optical nonlinearity of graphene, New J. Phys. **16**, 053014 (2014).
[32] W.-T. Liu, S. W. Wu, P. J. Schuck, M. Salmeron, Y. R. Shen, and F. Wang, Nonlinear broadband photoluminescence of graphene induced by femtosecond laser irradiation, Phys. Rev. B **82**, 081408 (2010).
[33] D. Huang *et al.*, Gate switching of ultrafast photoluminescence in graphene, Nano Lett. **18**, 7985 (2018).
[34] T. J. Constant, S. M. Hornett, D. E. Chang, and E. Hendry, All-optical generation of surface plasmons in graphene, Nat. Phys. **12**, 124 (2016).
[35] B. Yao *et al.*, Broadband gate-tunable terahertz plasmons in graphene heterostructures, Nat. Photonics **12**, 22 (2018).
[36] D. N. Basov, M. M. Fogler, A. Lanzara, F. Wang, and Y. B. Zhang, Colloquium: Graphene spectroscopy, Rev. Mod. Phys. **86**, 959 (2014).